Time-Dependent Stress Drop Variations After Large Earthquakes Along the North Chilean Megathrust

Jonas Folesky*[1] and Jörn Kummerow[1]

ABSTRACT

We observe a time dependence of the median stress drop in spatiotemporal proximity of large earthquakes. The median stress drop of the early aftershock seismicity is elevated for only a few days after the mainshocks and then rapidly falls back to the long-term average. This short-term variation has remained largely unnoticed by previous studies, presumably due to their usually low temporal resolution. Our study uses a recent extensive stress drop catalog, which contains more than 51,000 events from northern Chile. It includes observations from three $M_w > 7$ megathrust earthquakes, namely the 2007 M_w 7.7 Tocopilla earthquake, the 2014 M_w 8.1 Iquique earthquake, and its largest M_w 7.6 aftershock, as well as another eleven $M_w > 6$ earthquakes. A detailed analysis reveals that the elevated stress drop is not primarily linked to an increase of seismic moment during the early aftershock phase but is rather attributable to higher measured corner frequencies in the corresponding time interval. We propose two possible explanations: (1) The high stress changes induced by the mainshock allow failure of strong structures at or adjacent to the main rupture area, which produces higher stress drop events. After a few days, afterslip activity has reduced the in situ stresses and thereby the failure potential of the stronger regions. (2) The mainshock disturbs the fluid-sealing plate interface, allowing overpressured fluids to escape, exhibiting the so-called fault-valve behavior. The effect appears to persist only for several days until the sealing effect is restored and average stress drop levels are recovered.

KEY POINTS

- In the vicinity of the rupture zone, the average stress drop increases immediately after large earthquakes.
- The perturbation effect lasts for only a few days.
- Temporarily elevated stress drop may indicate failure of strong structures and/or fault-valve behavior at the plate interface.

Supplemental Material

INTRODUCTION

Stress drop is a source parameter that describes the relation of slip to the characteristic fault dimension of an earthquake (Brune, 1970, 1971; Shearer *et al.*, 2006). For real faults, it is affected in a complex way by fault strength, fault topography, the presence of fluids, stress state, and rupture velocity; that is, the stress drop is indicative of the hosting structure of the earthquake and the conditions under which it occurred (Goertz-Allmann *et al.*, 2011; Abercrombie, 2014, 2021; Kaneko and Shearer, 2014; Zielke *et al.*, 2017). High stress drop events feature an increased rate of high frequencies, making them more destructive to human infrastructure. The higher frequency content can have several origins. For example, the rupture surface can be rough, the fault can be young or previously intact (Zielke *et al.*, 2017), or the locking degree can be high (Allmann and Shearer, 2007). In contrast, low stress drops are rather found on mature faults, smoother or lubricated rupture surfaces (Goertz-Allmann *et al.*, 2011; Zielke *et al.*, 2017).

In general, the stress drop is computed as

$$\Delta\sigma = \frac{7\pi\mu\overline{D}}{16r} = \frac{7M_0}{16r^3} = \frac{7}{16}\left(\frac{f_c}{k\beta}\right)^3 M_0, \qquad (1)$$

in which μ is the rigidity, D is the average slip, r is the source radius, M_0 is the seismic moment, f_c is the corner frequency, the constant k relates to the spherical average of the corner frequency for a specific theoretical source model, and β is

1. Department of Geophysics, Freie Universität Berlin, Berlin, Germany, https://orcid.org/0000-0002-7729-9624 (JF); https://orcid.org/0000-0002-6026-5911 (JK)

*Corresponding author: jonas.folesky@geophysik.fu-berlin.de

Cite this article as Folesky, J., and J. Kummerow (2024). Time-Dependent Stress Drop Variations After Large Earthquakes Along the North Chilean Megathrust, *Bull. Seismol. Soc. Am.* **XX**, 1–11, doi: 10.1785/0120240121

the shear-wave velocity at the source used as a proxy for the rupture velocity (Abercrombie, 2014; Kaneko and Shearer, 2014; Pennington *et al.*, 2021). When variations of k and β are assumed to be small, the remaining parameters to investigate are M_0 and f_c. Because stress drop estimation is highly sensitive to the input parameters, errors can be high (Cotton *et al.*, 2013; Kaneko and Shearer, 2014; Abercrombie, 2021). Hence, the utilization of the large numbers of events is principally desirable, allowing the analysis of relative variability in the given data set rather than the comparison of absolute values originating in different studies (Shearer *et al.*, 2006; Abercrombie, 2021).

Large earthquakes are known to potentially alter the properties of not only their hosting fault(s) but also their direct surroundings, for example, by creating a damage zone (Rice *et al.*, 2005). Effects such as stress, friction, or velocity perturbations in a broader region have been described in multiple studies, for example, Rubinstein *et al.* (2007) and Kelly *et al.* (2013).

Most of the relatively few previous observations of time-dependent stress drop variations stem from medium-to-large-sized events or from induced seismicity. Importantly, the invoked causes are not unanimous and vary broadly between studies and their geological settings. For example, temporal stress drop variation was observed by spectral variations in repeating earthquakes at the San Andreas fault (Abercrombie, 2014). Following the 2004 M_w 6 Parkfield event, two out of three identified repeater series showed decreased stress drops closely after the main event occurrence. The authors explain this observation by the short healing time available between subsequent events. The effects revealed by earthquakes that repeatedly rupture an identical fault patch may, however, be of particular nature. Staszek *et al.* (2017) observed pore pressure-dependent stress drops in the Geysers geothermal field, California, where increased pore pressure led to a decrease of the estimated average stress drop. Moyer *et al.* (2018) studied the temporal stress drop variation at the Gofar Transform fault, East Pacific Rise, before and after an M_w 6 event in 2008. They found a month-long decrease of stress drop values and explained this by the damage zone that was created by the main event. According to them, increased attenuation could have decreased the apparent corner frequencies, causing the lower stress drop estimates. Allmann and Shearer (2007) analyzed stress drop changes at the San Andreas fault from before to after the 2004 M_w 6 Parkfield event using the spectral decomposition method (SDC) method (similar to the underlying method in this study). They found low stress drops for the creeping section of the fault and higher values for the locked part. Concerning the temporal variation, they only compared results from before to after the main event without finer temporal resolution and reported a small general increase, albeit spatial heterogeneity was the dominant factor. This increase, however, becomes apparent only after they have corrected for the postevent attenuation change separately. Trugman (2020) described stress drop variations after the 2019 M_w 7.1 Richcrest event using SDC-derived stress drops. They found elevated stress drop values for early aftershocks but observed that this might be an effect of the majority of early aftershocks being located in deeper sections of the fault. Kemna *et al.* (2021) discussed the stress drop of seismic sequences of the M_w 6 Amatrice and M_w 6.5 Norcia events in central Italy, 2016–2017. They reported an increased early aftershock stress drop, which recovers its preseismic average within weeks, and explained this by the release of short-term stress concentrations at formerly intact areas of high frictional strength adjacent to the mainshock slip area. They also indicate the possibility of a subsequent longer-lasting decrease of the stress drop, potentially caused by the damage zone that was inflicted by the main event, before returning to the long-term average.

The focus of this study lies on the temporal variation of Brune type stress drop (Brune, 1970, 1971) in the direct vicinity of large earthquakes in northern Chile. For this, the comprehensive stress drop catalog from Folesky *et al.* (2024) is searched for events neighboring the target mainshocks. The catalog covers 15 yr of data and consists of over 51,000 stress drop estimates, which allows a spatiotemporal resolution of stress drop variability from years to days. The three largest megathrust earthquakes that occurred in the covered time interval were the M_w 7.7 2007 Tocopilla earthquake (Schurr *et al.*, 2012), the M_w 8.1 Iquique earthquake, and its M_w 7.6 aftershock (Schurr *et al.*, 2014). Another eleven $M_w > 6$ events occurred at shallow depth (<70 km) in the observation period. Many of these large-magnitude events are accompanied by seismic sequences of fore- and aftershocks, which allows us to study the temporal variation of stress drop in the direct rupture vicinity in detail.

Because stress drop estimates are highly sensitive to the determined corner frequencies and seismic moments, we investigate in detail their contributing effects. The analysis is explained for the Iquique event because it was accompanied by the largest amount of seismicity, providing the most robust statistics. Subsequently, the analysis is extended to include the other two $M_w > 7$ earthquakes and all $M_w > 6$ events that occurred at or close to the plate boundary. After establishing the similarity of the observation for all analyzed events, two possible explanations for the observations are proposed.

DATA

The database for this work is the recent stress drop catalog of Folesky *et al.* (2024), who have computed 51,510 stress drops for an extensive seismicity catalog from northern Chile (Sippl *et al.*, 2023a). In a two-step approach, they applied first the spectral ratio technique for events in which suitable empirical Green's functions could be found by template matching. The obtained stress drop values were then used as a benchmark for the spectral decomposition approach, in which event spectra are corrected using an average Green's function, which is valid for a spatially limited region. Results from both methods were

compared to verify common patterns of stress drop variability throughout the subduction zone. Principally, the stress drop shows a log-normal distribution. About 97.5% of the estimates fall in the range between 0.1 and 100 MPa, and the stress drop shows scaling with magnitude, probably as a consequence of the processing choices such as the fixed $n = 2$ high-frequency falloff. For details, please see Folesky *et al.* (2024). Nonetheless, systematic differences in median stress drop between the different seismotectonic classes could be revealed; for example, plate interface events have on average lower stress drops than upper plate (UP) crustal seismicity or intermediate depth (ID) seismicity, a fact also observed by Derode and Campos (2019), who compared a small amount of shallow and ID events with a focus on stress drop, energy budget, and rupture velocity.

The catalog is ideal to investigate potential changes in stress drop over time because it covers a long time interval of 15 yr from 2007 to 2021. In this period, three major megathrust events occurred, namely the 2007 M_w 7.7 Tocopilla earthquake, the M_w 8.1 Iquique earthquake, and its M_w 7.6 aftershock. In addition, another eleven $M_w > 6$ events at or near the plate interface were observed. The mainshocks are partly not included in the stress drop catalog themselves, but their fore- and aftershock series are, which in the case of the Iquique event are extensive (Schurr *et al.*, 2014; Soto *et al.*, 2019). From the underlying seismicity catalog, we extract the event locations, magnitudes, and tectonic classification. Their listed calibrated magnitudes (M_A) are treated as moment magnitudes (M_w), as verified by Folesky *et al.* (2024). The stress drop estimation was done on 100 Hz z-component broadband data obtained at the IPOC seismic network (IPOC, 2006), limited to events with $M \geq 2$. Using a passband of 0.8–40 Hz, corner frequencies were searched in a range of 1–30 Hz. Stress drops were then computed using a regional 2D velocity model (Bloch *et al.*, 2014) and k values of $k_p = 0.32$ and $k_s = 0.265$, respectively. For about 90% of the events from the complete event catalog, stress drop values could be obtained. In this work, we restrict our analysis to stress drops from the seismotectonic event classes to which the mainshocks were associated, and we generally disregard mining-induced and ID seismicity. In northern Chile, at ID, about 80% of the total seismicity is recorded. Consequentially, the utilized catalog for this study reduces to 6718 natural events of magnitude 2–6.4. The majority of mainshocks occurred at the plate interface events and thus are part of the interface class (P1). The upper plane of the double seismic zone (P2) only hosts one of the major events, and none is found in class of lower plane (P3) or UP. Two large events from this work are located in the NN class, which is simply describing areas of the least spatial resolution at the catalog rim. The spatial distribution of the stress drop, the megathrust event hypocenters, and the available slip contours of the three largest earthquakes are shown in Figure 1. In addition, the figure shows histograms of stress drop, corner frequency, and magnitudes for the utilized sub-catalog as well as for each event class, separately. Here, the principally higher stress drop values in the UP (mostly crustal seismicity) and the generally lower stress drops along the entire interface can be seen. Also, the spatial heterogeneity of the stress drop distribution becomes apparent; see, for example, the region at the southern bound of the high slip patch of the Iquique event at around 20°S. For further details on the methods of computing the stress drop and on their errors and limitations, we refer to the original publication.

OBSERVATIONS

We start with isolating the seismicity around the major event's slip area. Next, the stress drops are split into three distinct groups: (I) foreshocks, (II) immediate aftershocks, and (III) later aftershocks, as shown exemplarily for the M_w 8.1 Iquique earthquake in Figure 2. The corresponding event locations for the Iquique mainshock are shown in Figure S8, available in the supplemental material to this article. The selected time intervals for groups I, II, and III are 14, 5, and 35 days, respectively. Events outside the analysis windows are only considered for calculating the long-term stress drop median, which is based on all available stress drop estimates in the target area. For the Iquique earthquake, we then compute a short-term stress drop median to observe its potential variability by taking the median of the stress drop estimates over 60 consecutive events with a step increment of 5 events. This short-term stress drop median is clearly elevated in the early aftershock period. During this time interval, we find values of 3–4 MPa, whereas foreshocks and later aftershocks both show lower values, close to the long-term median of 1.29 MPa of that region. The here observed stress drop perturbation is the strongest in the entire 15-yr-long time series (Folesky *et al.*, 2024) in the Iquique event rupture region. The same observation was reported by Folesky *et al.* (2021), who studied stress drop variations solely based on spectral ratio estimates in the same region.

The two previously mentioned studies already showed that the temporarily increased moment release, that is, on average higher magnitude events, contributed to the observed elevated stress drop values. Here, we additionally investigate the effect of an elevated corner frequency. For this, the source spectra of all events from the M_w 8.1 Iquique seismic series are displayed in small $\Delta M = 0.2$ magnitude bins in Figure 3, colored corresponding to their associated time interval. Each spectrum represents the average over all contributing stations. The spectra are corrected for attenuation, site, and path responses (Folesky *et al.*, 2024). They, therefore, ideally represent only the source spectra. For each group, the median of the corner frequency of all spectra is indicated by a vertical line. The figure shows that for almost all magnitude bins containing more than 10 spectra per class (all bins between M_w 2 and 3.8), the median corner frequency is consistently elevated for the early aftershock events. Therefore, the increased corner frequencies also account for the observed stress drop increase during the

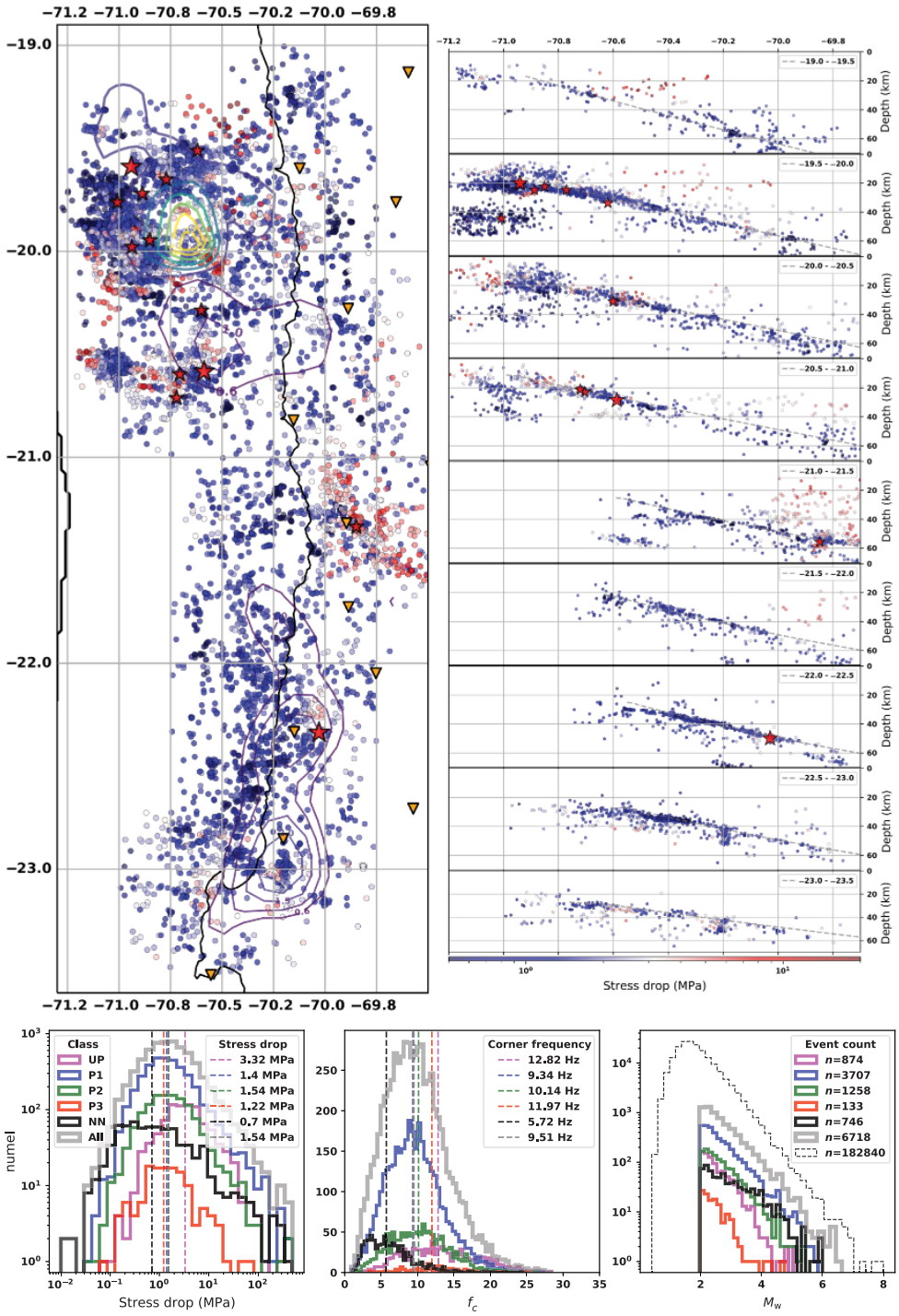

Figure 1. Stress drop distribution map view and east–west depth slices for 0.5° latitudinal bins for events shallower than 70 km. Coloring is blue to red for low to high stress drops, respectively. The stress drop is smoothed by computing the median over the 10 nearest neighbors. Orange triangles depict the IPOC (2006) seismic stations. Red stars are $M_w > 6$ events in the target region, where the largest three stars, from north to south, are the hypocenters of the M_w 8.1 2014 Iquique event, its biggest M_w 7.6 aftershock, and the M_w 7.7 2007 Tocopilla event, which are complemented by their slip contours (Schurr *et al.*, 2012, 2014; Duputel *et al.*, 2015). The thin gray-dashed line is the plate interface estimated by Sippl *et al.* (2018). The principally low stress drop of the interface seismicity interrupted by locally strongly elevated values is clearly seen. The bottom row shows histograms for stress drops, corner frequency, and magnitudes, separated for the different occurrence regions (see Data section).

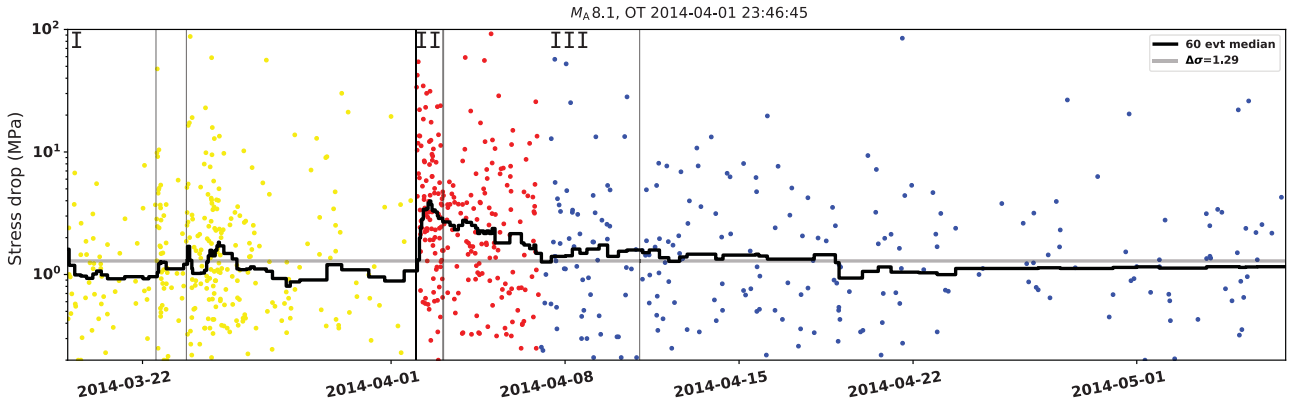

Figure 2. Stress drops versus time in the vicinity of the 2014 M_w 8.1 Iquique origin. Fourteen days of preseismic events (I) are colored yellow, five days of early aftershocks (II) are colored red, and five weeks of later aftershocks (III) are colored blue. The correspondingly colored event locations are shown in Figure S8. The gray horizontal line is the long-term median ($\Delta\sigma = 1.29$ MPa). Thin vertical black lines denote occurrences of other large ($M_w > 6$) events. Overlain in black is the 60-event stress drop median, calculated every 5 events. It reveals a significant increase of stress drop in the early aftershock period (red) and a following rapid decrease.

early aftershock period. The observation of a temporal increase of corner frequency that is persistent in all well-sampled magnitude bins reveals the across-scale nature of the effect, and simultaneously it means that the scaling between magnitude and stress drop is not the source of the effect. In fact, the smaller magnitude events contribute much more strongly to the effect, simply by virtue of their greater numbers.

We repeat the analysis described here for the M_w 7.7 Tocopilla event and for the M_w 7.6 aftershock of the Iquique event. Their median stress drop curves are shown in Figure 4. The corresponding map views are displayed in Figures S1 and S11. The corresponding magnitude bin-separated source spectra can be found in Figures S15 and S16. We observe a qualitatively similar behavior of the median stress drop: In the early aftershock period, the median stress drop is increased. After a few days, stress drop falls back to the long-term median value.

Next, we extend the analysis to the $M_w > 6$ events from the IPOC catalog, which are located at or close to the plate interface and which are shallower than 70 km. For each of these large events, we select all neighboring events of the same tectonic class within a radius of 25 km around its hypocenter. After classification into the temporal units (I/II/III), as described for the Iquique seismic sequence, we observe similar curves of median stress drop variation as found for the larger events. Amplitude and duration of the short-term median stress drop increase are smaller than for the larger events, but for eight out of eleven events the observation can be confirmed. The results for all events are summarized in Table 1, and the median stress drop curves for all events that show the effect are plotted in Figure 5. For the remaining three events, it is not possible to examine the effect because they do not have enough associated seismicity or not enough stress drop estimates in their direct vicinity to observe stress drop variations robustly. The individual stress drop curves for all analyzed events and the map views illustrating each seismic sequence are shown in Figures S1–S14.

DISCUSSION

The principal observation described in this work is the occurrence of a short-term elevation of the median stress drop level immediately following large $M_w > 6$ mainshocks in northern Chile. The effect is observed for time periods of up to six days. The responsible process must consequentially be highly dynamic. We propose two possible hypotheses that can explain the observations. Both will be discussed in the following.

High fault strength

One possible explanation of increased stress drop is based on the intrinsic heterogeneity of fault structures as indicated by stress drop estimates, for example, by Ruhl *et al.* (2017). Along the northern Chilean megathrust, lateral variations of stress drop were recently described in detail by Folesky (2024). The 2014 M_w 8.1 Iquique event ruptured a 100–150-km-long part of the northern Chilean seismic gap. After about 27 hr, it was followed by its largest M_w 7.6 aftershock. Detailed slip inversion and rupture directivity studies resolved that the rupture of the M_w 8.1 Iquique earthquake progressed from the hypocenter in the north toward the southeast (Schurr *et al.*, 2014; Folesky *et al.*, 2018), with a concentration of slip occurring during the later rupture phase in the southeast (Duputel *et al.*, 2015). Farther south, the rupture came to a halt. It is plausible to assume that structural limitations inhibited the rupture from propagating farther south. Independently, Soto *et al.* (2019) identified repeating earthquakes and streaklike structures that align east–west at the latitudes of the southern edge of the rupture at about 20.2°S. Repeaters are known to occur on stronger asperities that are surrounded by weaker creeping sections. Using active seismics in combination with gravimetric measurements (Storch *et al.*, 2023) found that the Iquique earthquake was located in a

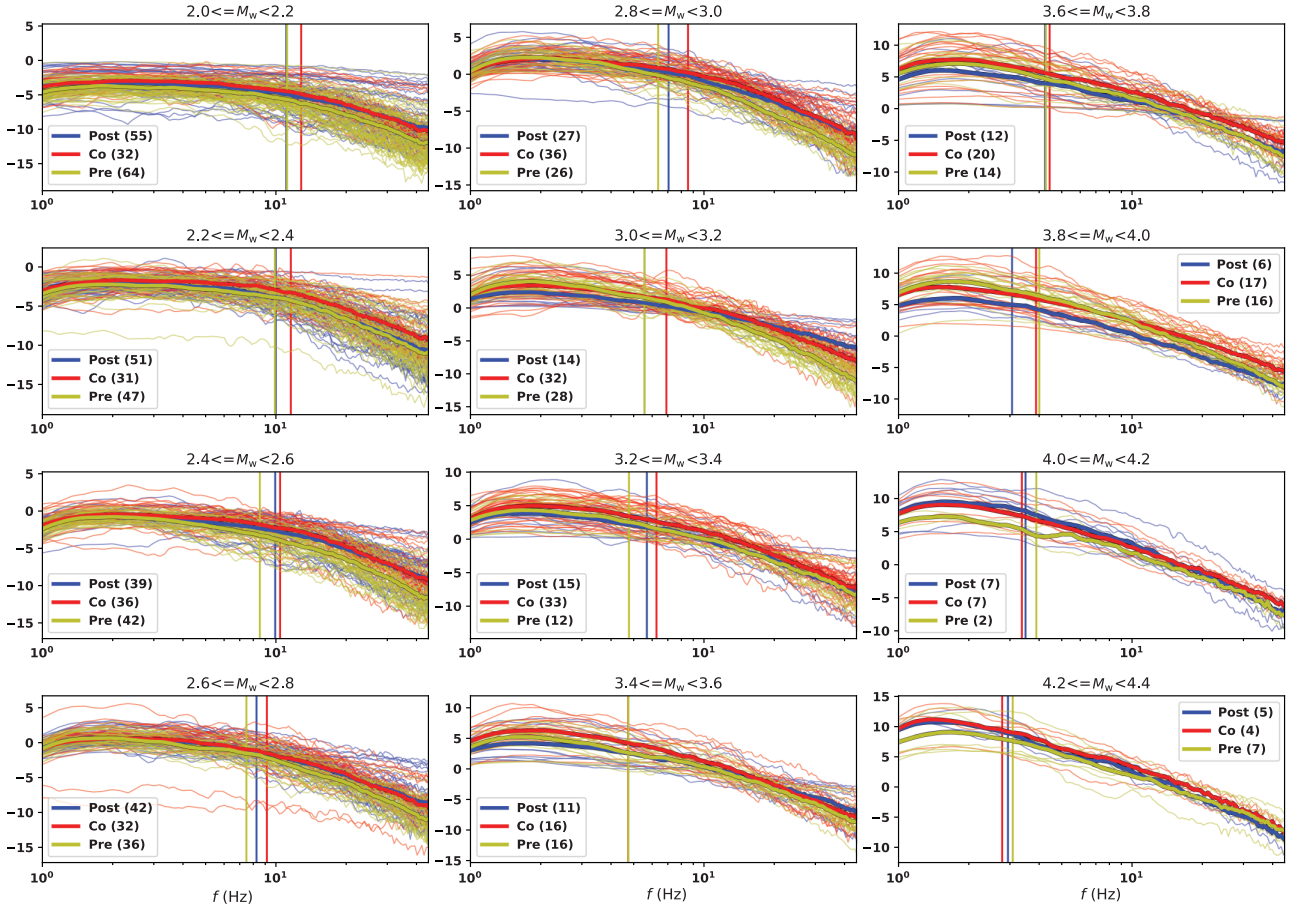

depression on the plate interface separated by a topographic high from the large M_w 7.6 aftershock. This west–east-striking topographic barrier might also have stopped the rupture. Apparently, the stress perturbation needed about one day to overcome this barrier until the large aftershock occurred. It is likely that this topographically elevated part of the interface differs from the depression, for example, through increased coupling, that is, higher yield strength. Indeed, the early aftershock phase shows a concentration of events at the southern rim of the slip region, and their stress drops are high (Fig. 6, gray-dashed ellipsoids).

The large stress change inflicted by the main event could have allowed it to overcome the criticality threshold for potential events on this region of high fault strength. Comparison to Coulomb failure stress change (Soto *et al.*, 2019) suggests that either areas with the highest resulting stress change or areas with the highest spatial gradient of the stress change may produce the highest stress drop events. The effect decays rapidly, as afterslip reduces the stress perturbation successively (Itoh *et al.*, 2023). After five days, the potential to activate the stronger fault patches has largely ceased, and event rates decrease at these particular sites (Fig. 6, gray-dashed ellipsoids, phases II–III).

Figure 3. Source spectra obtained from the spectral decomposition procedure as described in Folesky *et al.* (2024). Each line represents the *P*-phase-derived source spectrum after removing path, instrument, and site response (the empirical Green's functions [EGF] method) and averaging for all contributing stations. The spectra are binned for $\Delta M = 0.2$. Color corresponds to occurrence time indicating the event groups: (I, pre) foreshocks, (II, co) immediate aftershocks, and (III, post) later aftershocks (Fig. 2). For each bin, the average corner frequency is indicated by a vertical line. The thicker spectrum is the average for that bin and event group. There are 45 events with $M_w > 4.4$ the spectra of which are not shown. For almost all bins with more than 10 events per group, the red line (immediate aftershocks) indicates a higher median corner frequency than for the other two groups.

Fault-valve effect

On the other hand, we also observe variable stress drops in areas that are active during part or all of the three time periods. Two example regions are highlighted in Figure 6 encircled by black-dashed curves. Events in the western region are predominately of low stress drop in the foreshock (I) and aftershock period (III), and they clearly exhibit higher stress drops in the early aftershock time (II). In the region marked by the southeastern ellipsoid, seismicity is absent in phase but again shows clearly higher stress drops in phase II than in phase III.

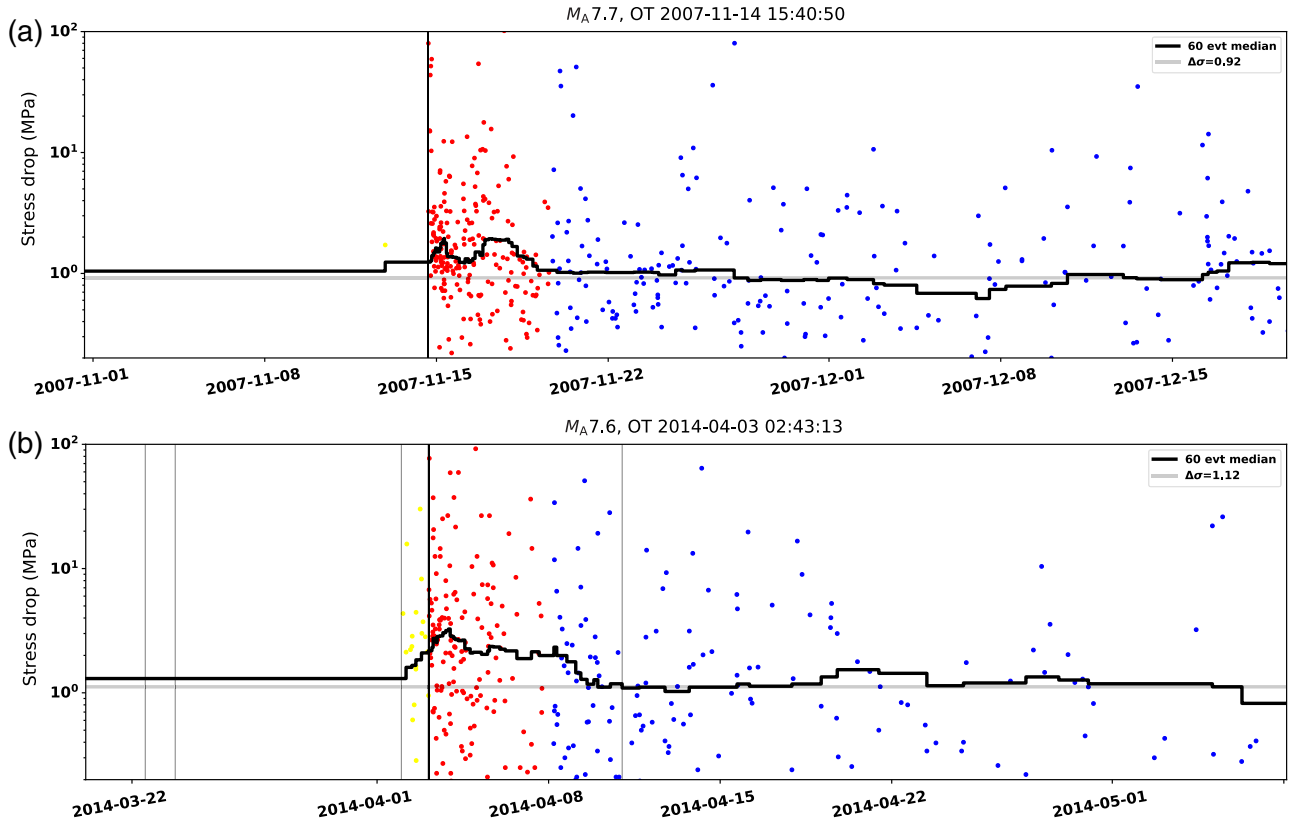

Figure 4. Stress drop versus time similar to Figure 2 but for the M_w 7.7 Tocopilla earthquake (a) and for the M_w 7.6 Iquique event aftershock (b). The corresponding seismicity maps are shown in Figures S1 and S11. Albeit their smaller sizes compared to the Iquique mainshock, both events are followed by a median stress drop increase just after the mainshock, followed by a clear drop after about five days. Gray vertical lines indicate other large events in the temporal vicinity of the mainshock that may have caused additional stress perturbations, such as the Iquique event one day before the large aftershock. The color version of this figure is available only in the electronic edition.

Such a temporal alteration suggests a change of fault properties rather than the activation of different fault patches, as proposed in the previous paragraph for the segment at the southeastern end of the mainshock rupture area.

One possible mechanism that could have produced the observed stress drop variation is a redistribution of fluids on the interface, in particular by the fault-valve effect (Sibson, 1990). Subduction interface megathrusts are one of the prime candidates for the complex interaction of increasing differential stress and pore-fluid pressure (Sibson, 2020). The overpressurized fluid that is locked in a given region is released by the seismic event. The earthquake breaks or damages the seal, fluid pressure drops rapidly, and the friction coefficient increases accordingly. Resealing of the opened fluid pathways begins instantly as fluid is transported through the leak and minerals fall out of the less pressurized fluid. When the healing from hydrothermal cementation has reduced fault permeability sufficiently, fluid pressure begins to build up again. During this phase, the stress perturbation on local asperities inflicted by the mainshock is maximal, which should suffice to activate potential source regions, albeit the frictional strengthening effect of the fluid pressure drop. The events in this time window would then exhibit an increased stress drop.

In our case, the plate interface itself could have constituted the impermeable seal. Reportedly, fault cores often act as impermeable fluid barriers (Bense *et al.*, 2013). A large event might have damaged this seal considerably. The observed topographic depression described by Storch *et al.* (2023) could provide the lateral limits of the affected area. The fluid may escape into the UP or redistribute along the interface. Apparently the process is highly dynamic, and its effect on the recorded event stress drop lasts for only up to six days for the Iquique event. For the corresponding period, we observe that the crustal stress drop in the UP shows weak evidence for a temporal decrease, which would support an upward fluid migration that affects crustal seismicity there by lowering effective stress and thus reducing the stress drop. In the following days, more aftershocks occur on similar or adjacent fault segments on the interface, now favored additionally by the buildup of the fluid pressure. Their stress drops show on average the restored long-term median stress drop level.

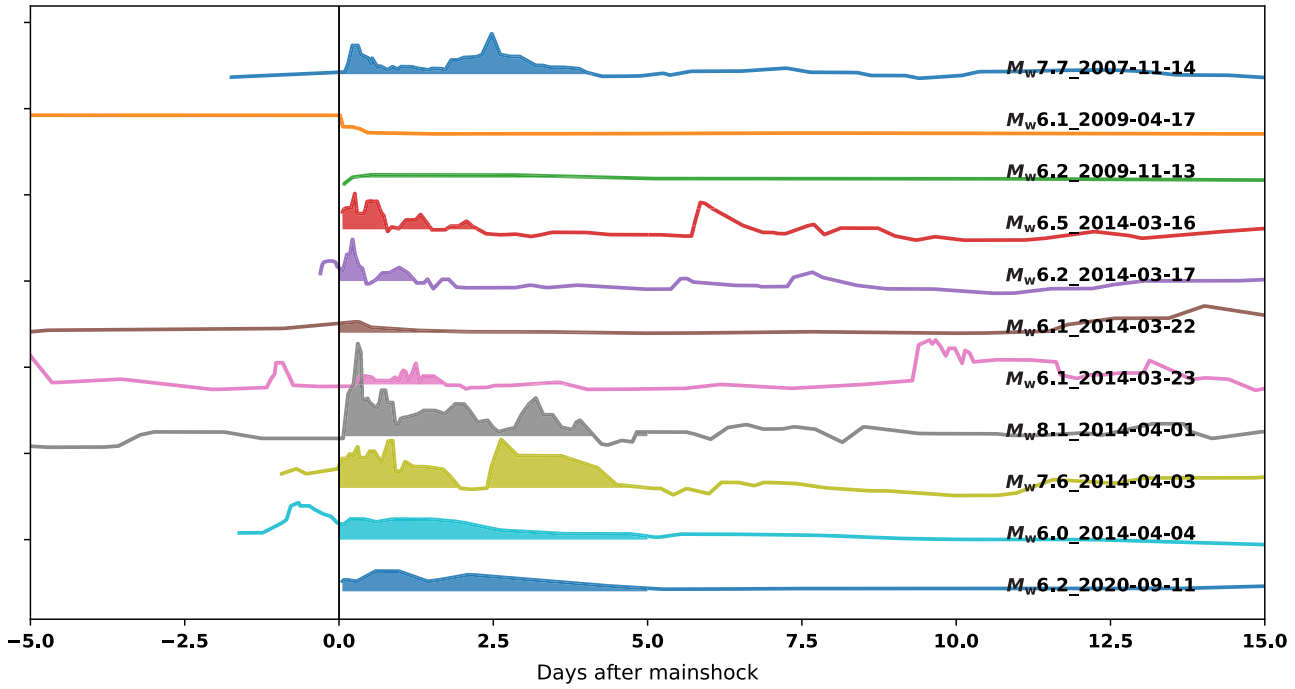

Figure 5. Median stress drop versus time curves for eleven $M_w > 6$ events. For all events, the colored lines indicate the median stress drop curve calculated for 25 successively occurring events, plotted with a 5-event increment (80% overlap). Each curve is corrected by the long-term median of the source region. Events are aligned by their origin time. For the first five days, the area under the curves is filled to better illuminate the positive perturbation of median stress drop during that time period. All nine mainshocks are followed by a period of elevated stress drop that decays swiftly in a matter of days. Also, additional spikes of stress drop may occur at other times. These spikes are caused by other large event occurrences in the respective target areas. All detailed individual curves and corresponding seismicity maps are plotted in Figures S1–S14. The color version of this figure is available only in the electronic edition.

TABLE 1
Chronological List of $M_w > 6$ Events from This Study, with $M_w > 7$ in Bold

S. No.	Time (yyyy/mm/dd hh:mm:ss)	Latitude (°)	Longitude (°)	Depth (km)	Magnitude (M_w)	Class	$\frac{\Delta\sigma_{max}}{\Delta\sigma}$	t_{elev}
1	**2007/11/14 15:40:50**	**−22.34**	**−70.03**	**49.95**	**7.7**	**P1**	**3.5**	**5**
2	2009/04/17 02:08:07	−19.65	−70.77	24.92	6.1	P1	1.5	0.5
3	2009/11/13 03:05:57	−19.51	−70.62	33.8	6.2	P1	1.2	2
4	2010/05/06 02:42:47	−18.22	−70.91	46.14	6.1	NN	–	–
5	2014/03/16 21:16:29	−19.95	−70.85	22.46	6.5	P1	2.6	3
6	2014/03/17 05:11:34	−19.98	−70.94	21.16	6.2	P1	2.8	2
7	2014/03/22 12:59:59	−19.76	−71.01	44.5	6.1	NN	2.4	3
8	2014/03/23 18:20:01	−19.72	−70.89	24.82	6.1	P1	2.1	2
9	**2014/04/01 23:46:45**	**−19.59**	**−70.94**	**19.91**	**8.1**	**P1**	**5.2**	**5**
10	2014/04/03 01:58:31	−20.29	−70.60	31.11	6.2	P2	–	–
11	**2014/04/03 02:43:13**	**−20.58**	**−70.59**	**28.47**	**7.6**	**P1**	**3.5**	**6**
12	2014/04/04 01:37:51	−20.60	−70.70	22.99	6.0	P1	2.1	5
13	2014/04/11 00:01:45	−20.71	−70.72	21.12	6.1	P1	–	–
14	2020/09/11 07:35:56	−21.34	−69.85	55.76	6.2	P1	2.2	4

Columns 2–7 were taken from Sippl *et al.* (2023a,b). $\frac{\Delta\sigma_{max}}{\Delta\sigma}$ is the maximum short-term stress drop level increase factor found within five days after the mainshock, computed from the 25 events average (see the Methods section), relative to the local long-term median. t_{elev} is the approximate duration of median stress drop elevation in days. For each event, the median stress drop curve and the corresponding map of the seismicity from the source region are shown in the supplemental material for individual inspection.

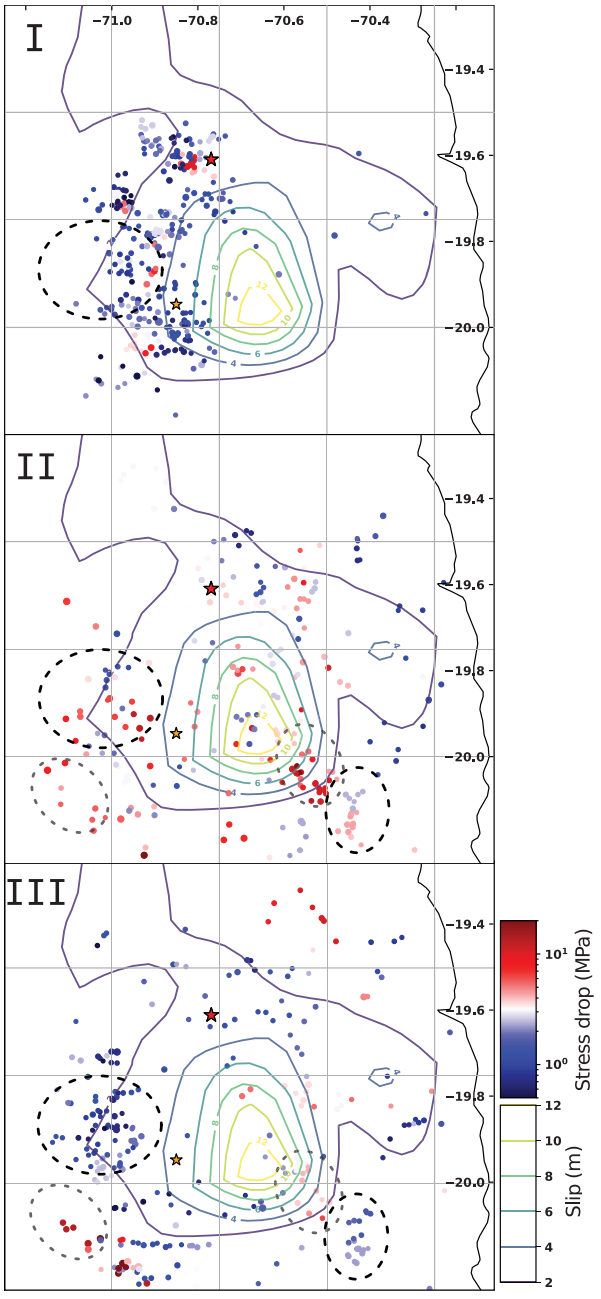

Figure 6. Locations and stress drops of (I) foreshocks, (II) early aftershocks, and (III) later aftershocks of the 2014 M_w 8.1 Iquique event. Stress drops are smoothed over 10 nearest neighbors, blue to red for low to high values, respectively. Slip contour from Duputel *et al.* (2015). Red star and orange star are epicenters of the M_w 8.1 Iquique event and its largest foreshock (2 weeks earlier, 17 March 2014 05:11:34). The foreshock series (I) was located west of the main slip patch. The events are predominately of low stress drop, with highly localized exceptions, for example, close to the later Iquique event hypocenter. Early aftershocks (II) cover the entire slip area and display high stress drop, especially in the south. Later aftershocks (III) progress farther outward with again lower stress drop values, except at the very southwest and northeast. Dashed ellipsoids mark regions of variable stress drop (gray line) and stable, elevated stress drop (black line), which are further discussed in the Discussion section.

CONCLUSION

A recent comprehensive stress drop catalog for northern Chile containing tens of thousands of stress drop estimates for the years 2007–2021 allows the analysis of local time-dependent stress drop variability with a resolution of several days. We observe an elevated average stress drop level for a short time period of a few days after the occurrences of the three recorded megathrust earthquakes and several $M > 6$ earthquakes. The stress drop increases are in the order of 80%–200% and are the highest stress drop deviations from the median during the entire observation period within the corresponding regions. The predominant effect responsible for the elevated stress drop is an increased average corner frequency relative to their seismic moment for the events that occurred during the early aftershock period.

Multiple processes and their interactions may lead to an increase of the median stress drop. We discuss two potential processes. First, high local stress perturbations in the time period after the megathrust occurrence may activate stronger seismogenic structures. For the M_w 8.1 Iquique earthquake, this is evidenced by high stress drop events that cluster close to the large slip segment at the southern end of the mainshock rupture. This effect decreases rapidly as afterslip reduces the differential stresses. A second mechanism that can produce higher stress drop events is the fault-valve effect, in which the overpressurized fluids that are trapped by the impermeable seal at the plate interface are released by the megathrust event. This causes a short period of fluid pressure drop until the sealing is restored. During that time, friction is elevated, and all events that do occur potentially show a higher stress drop.

If the latter were the case, this study would constitute an unprecedentedly direct observation of the fault-valve behavior at the megathrust, and it would put new constraints on the time window in which the effect is active.

DATA AND RESOURCES

The northern Chile seismic catalog (Sippl *et al.*, 2023a) is available at doi: 10.5880/GFZ.4.1.2023.004; the stress drop catalog (Folesky *et al.*, 2024) is available at doi: 10.5281/zenodo.10400960; and the source spectra are available upon request from the corresponding author. Processing was performed in Python 3.7 using NumPy (Harris *et al.*, 2020) v.1.21.6, pandas (pandas development team, 2020) v.1.3.4, ObsPy (Beyreuther *et al.*, 2010) v.1.2.2, and sklearn (Pedregosa *et al.*, 2011) v.1.0.2. The plots were created using Matplotlib (Hunter, 2007) v.3.5.1 and cartopy (Met Office, 2010–2015) v.0.20.2. for maps. The supplemental material to this article includes the seismic sequences of each of the large events discussed in the article and listed in Table 1, alongside their stress drop estimates and the median stress drop curves (Figs. S1–S12).

DECLARATION OF COMPETING INTERESTS

The authors acknowledge there are no conflicts of interest recorded.

ACKNOWLEDGMENTS

J. F. was funded by the German Science Foundation (DFG), Project Numbers FO 1325/2-1 and FO 1325/3-1. The authors want to thank the reviewers and the editor T. Uchide for helping to improve this article.

REFERENCES

Abercrombie, R. E. (2014). Stress drops of repeating earthquakes on the San Andreas fault at Parkfield, *Geophys. Res. Lett.* **41,** no. 24, 8784–8791.

Abercrombie, R. E. (2021). Resolution and uncertainties in estimates of earthquake stress drop and energy release, *Philos. Trans. R. Soc. A* **379,** no. 2196, 20200131, doi: 10.1098/rsta.2020.0131.

Allmann, B. P., and P. M. Shearer (2007). Spatial and temporal stress drop variations in small earthquakes near Parkfield, California, *J. Geophys. Res.* **112,** no. B4, doi: 10.1029/2006JB004395.

Bense, V., T. Gleeson, S. Loveless, O. Bour, and J. Scibek (2013). Fault zone hydrogeology, *Earth Sci. Rev.* **127,** 171–192.

Beyreuther, M., R. Barsch, L. Krischer, T. Megies, Y. Behr, and J. Wassermann (2010). ObsPy: A Python toolbox for seismology, *Seismol. Res. Lett.* **81,** no. 3, 530–533.

Bloch, W., J. Kummerow, P. Salazar, P. Wigger, and S. Shapiro (2014). High-resolution image of the north Chilean subduction zone: Seismicity, reflectivity and fluids, *Geophys. J. Int.* **197,** no. 3, 1744–1749.

Brune, J. N. (1970). Tectonic stress and the spectra of seismic shear waves from earthquakes, *J. Geophys. Res.* **75,** no. 26, 4997, doi: 10.1029/JB075i026p04997.

Brune, J. N. (1971). Seismic sources, fault plane studies and tectonics, *EOS Trans. AGU* **52,** no. 5, IUGG-178.

Cotton, F., R. Archuleta, and M. Causse (2013). What is sigma of the stress drop? *Seismol. Res. Lett.* **84,** no. 1, 42–48.

Derode, B., and J. Campos (2019). Energy budget of intermediate-depth earthquakes in northern Chile: Comparison with shallow earthquakes and implications of rupture velocity models used, *Geophys. Res. Lett.* **46,** no. 5, 2484–2493.

Duputel, Z., J. Jiang, R. Jolivet, M. Simons, L. Rivera, J. P. Ampuero, B. Riel, S. E. Owen, A. W. Moore, S. V. Samsonov, *et al.* (2015). The Iquique earthquake sequence of April 2014: Bayesian modeling accounting for prediction uncertainty, *Geophys. Res. Lett.* **42,** no. 19, 7949–7957.

Folesky, J. (2024). Different earthquake nucleation conditions revealed by stress drop and b-value mapping in the northern Chilean subduction zone, *Sci. Rep.* **14,** 12182. doi: 10.1038/s41598-024-63015-w

Folesky, J., J. Kummerow, G. Asch, B. Schurr, C. Sippl, F. Tilmann, and S. Shapiro (2018). Estimating rupture directions from local earthquake data using the IPOC observatory in northern Chile, *Seismol. Res. Lett.* **89,** no. 2A, 495–502.

Folesky, J., J. Kummerow, and S. A. Shapiro (2021). Stress drop variations in the region of the 2014 MW8.1 Iquique earthquake, northern Chile, *J. Geophys. Res.* **126,** no. 4, e2020JB020112, doi: 10.1029/2020JB020112.

Folesky, J., C. Pennington, J. Kummerow, and L. Hofman (2024). A comprehensive stress drop map from trench to depth in the northern Chilean subduction zone, *J. Geophys. Res.* **129,** no. 1, e2023JB027549, doi: 10.1029/2023JB027549.

Goertz-Allmann, B. P., A. Goertz, and S. Wiemer (2011). Stress drop variations of induced earthquakes at the Basel geothermal site, *Geophys. Res. Lett.* **38,** no. 9, doi: 10.1029/2011GL047498.

Harris, C. R., K. J. Millman, S. J. Van Der Walt, R. Gommers, P. Virtanen, D. Cournapeau, E. Wieser, J. Taylor, S. Berg, N. J. Smith, *et al.* (2020). Array programming with NumPy, *Nature* **585,** no. 7825, 357–362.

Hunter, J. D. (2007). Matplotlib: A 2d graphics environment, *Comput. Sci. Eng.* **9,** no. 3, 90–95.

IPOC (2006). IPOC seismic network. Integrated Plate boundary Observatory Chile - IPOC, *GFZ German Research Centre for Geosciences*, Institut des Sciences de l'Univers-Centre National de la Recherche CNRS-INSU, Seismic Network (Vol. Seismic Network), doi: 10.14470/PK615318.

Itoh, Y., A. Socquet, and M. Radiguet (2023). Largest aftershock nucleation driven by afterslip during the 2014 Iquique sequence, *Geophys. Res. Lett.* **50,** no. 24, e2023GL104852, doi: 10.1029/2023GL104852.

Kaneko, Y., and P. M. Shearer (2014). Seismic source spectra and estimated stress drop derived from cohesive-zone models of circular subshear rupture, *Geophys. J. Int.* **197,** no. 2, 1002–1015, doi: 10.1093/gji/ggu030

Kelly, C., A. Rietbrock, D. Faulkner, and R. Nadeau (2013). Temporal changes in attenuation associated with the 2004 m6. 0 Parkfield earthquake, *J. Geophys. Res.* **118,** no. 2, 630–645.

Kemna, K. B., A. Verdecchia, and R. M. Harrington (2021). Spatiotemporal evolution of earthquake static stress drop values in the 2016-2017 central Italy seismic sequence, *J. Geophys. Res.* **126,** no. 11, e2021JB022566, doi: 10.1029/2021JB022566.

Met Office (2010–2015). Cartopy: A cartographic Python library with a Matplotlib interface [Computer software manual], Exeter, Devon, available at https://scitools.org.uk/cartopy/docs/latest/citation.html (last accessed October 2024).

Moyer, P. A., M. S. Boettcher, J. J. McGuire, and J. A. Collins (2018). Spatial and temporal variations in earthquake stress drop on Gofar transform fault, east pacific rise: Implications for fault strength, *J. Geophys. Res.* **123,** no. 9, 7722–7740.

pandas development team (2020). pandas-dev/pandas: Pandas, *Zenodo*, doi: 10.5281/zenodo.3509134.

Pedregosa, F., G. Varoquaux, A. Gramfort, V. Michel, B. Thirion, O. Grisel, M. Blondel, P. Prettenhofer, R. Weiss, V. Dubourg, *et al.* (2011). Scikit-learn: Machine learning in Python, *J. Mach. Learn. Res.* **12,** 2825–2830.

Pennington, C. N., X. Chen, R. E. Abercrombie, and Q. Wu (2021). Cross validation of stress drop estimates and interpretations for the 2011 Prague, OK, earthquake sequence using multiple methods, *J. Geophys. Res.* **126,** no. 3, e2020JB020888, doi: 10.1029/2020JB020888.

Rice, J. R., C. G. Sammis, and R. Parsons (2005). Off-fault secondary failure induced by a dynamic slip pulse, *Bull. Seismol. Soc. Am.* **95,** no. 1, 109–134.

Rubinstein, J. L., N. Uchida, and G. C. Beroza (2007). Seismic velocity reductions caused by the 2003 Tokachi-Oki earthquake, *J. Geophys. Res.* **112,** no. B5, doi: 10.1029/2006JB004440.

Ruhl, C., R. Abercrombie, and K. Smith (2017). Spatiotemporal variation of stress drop during the 2008 mogul, Nevada, earthquake swarm, *J. Geophys. Res.* **122,** no. 10, 8163–8180.

Schurr, B., G. Asch, S. Hainzl, J. Bedford, A. Hoechner, M. Palo, R. Wang, M. Moreno, M. Bartsch, Y. Zhang, *et al.* (2014). Gradual unlocking of plate boundary controlled initiation of the 2014 Iquique earthquake, *Nature* **512,** no. 7514, 299.

Schurr, B., G. Asch, M. Rosenau, R. Wang, O. Oncken, S. Barrientos, P. Salazar, and J. P. Vilotte (2012). The 2007 m7.7 Tocopilla northern Chile earthquake sequence: Implications for along-strike and downdip rupture segmentation and megathrust frictional behavior, *J. Geophys. Res.* **117,** no. B5, doi: 10.1029/2011JB009030.

Shearer, P. M., G. A. Prieto, and E. Hauksson (2006). Comprehensive analysis of earthquake source spectra in southern California, *J. Geophys. Res.* **111,** no. B6, doi: 10.1029/2005JB003979.

Sibson, R. H. (1990). *Conditions for Fault-Valve Behavior*, Vol. 54, Geological Society, London, Special Publications, 15–28.

Sibson, R. H. (2020). Dual-driven fault failure in the lower seismogenic zone, *Bull. Seismol. Soc. Am.* **110,** no. 2, 850–862.

Sippl, C., B. Schurr, G. Asch, and J. Kummerow (2018). Seismicity structure of the northern Chile forearc from >100,000 double-difference relocated hypocenters, *J. Geophys. Res.* **123,** no. 5, 4063–4087.

Sippl, C., B. Schurr, J. Münchmeyer, S. Barrientos, and O. Oncken (2023a). Catalogue of earthquake hypocenters for northern Chile from 2007-2021 using IPOC (plus auxiliary) seismic stations, *GFZ Data Services*, doi: 10.5880/GFZ.4.1.2023.004.

Sippl, C., B. Schurr, J. Münchmeyer, S. Barrientos, and O. Oncken (2023b). The northern Chile forearc constrained by 15 years of permanent seismic monitoring, *J. South Am. Earth Sci.* **126,** 104326.

Soto, H., C. Sippl, B. Schurr, J. Kummerow, G. Asch, F. Tilmann, D. Comte, S. Ruiz, and O. Oncken (2019). Probing the northern Chile megathrust with seismicity: The 2014 M8. 1 Iquique earthquake sequence, *J. Geophys. Res.* **124,** no. 12, 12,935–12,954.

Staszek, M., B. Orlecka-Sikora, K. Leptokaropoulos, G. Kwiatek, and P. Martínez-Garzón (2017). Temporal static stress drop variations due to injection activity at the geysers geothermal field, California, *Geophys. Res. Lett.* **44,** no. 14, 7168–7176.

Storch, I., S. Buske, P. Victor, and O. Oncken (2023). A topographic depression on the subducting Nazca plate controls the April 1st 2014 m8. 1 Iquique earthquake rupture in northern Chile, *Tectonophysics* **847,** 229684.

Trugman, D. T. (2020). Stress-drop and source scaling of the 2019 Ridgecrest, California, earthquake sequence, *Bull. Seismol. Soc. Am.* **110,** no. 4, 1859–1871.

Zielke, O., M. Galis, and P. M. Mai (2017). Fault roughness and strength heterogeneity control earthquake size and stress drop, *Geophys. Res. Lett.* **44,** no. 2, 777–783.

Manuscript received 14 June 2024
Published online 6 November 2024